Journal of Statistical Physics, Vol. 41, No. 1/2, 1985

Transitions Tori-Chaos Through Collisions with Hyperbolic Orbits

Giovanni Riela[1]

Received February 8, 1984; final January 21, 1985

Three models of dissipative dynamical systems are described in which a transition from biperiodic to aperiodic motion proceeds via collisions of a hyperbolic orbit with either a torus or a strange attractor.

KEY WORDS: Dissipative systems; breakdown of tori; strange attractors.

1. INTRODUCTION

The problem of transition to chaos in dynamical systems has received in the last few years a lot of interest. It has been studied extensively both from the theoretical and the experimental or numerical point of view. Many "scenarios" in which chaos is reached from periodic regimes are by now well established in very many experimental or numerical works carried out on a large variety of physical systems and mathematical models; they are also fairly well understood theoretically (see Refs. 1–4). This is not the case for transitions to chaos from doubly periodic regimes: even though this route to chaos is rather frequently seen in physical systems and the theoretical literature on the subject is growing rapidly, a satisfactory understanding of the matter has not yet been achieved.

Among the scenarios so far encountered in studies of the break-up of invariant circles in two dimensions or of two-dimensional invariant tori in higher-dimensional systems we mention (a) doubling of tori (Refs. 5–8), (b) oscillations between a couple of tori symmetrically conjugate of each other (Refs. 9–10), (c) occurrence of homoclinic tangency (Refs. 11, 12). In a number of other cases it seems that the transition to chaos occurs through

[1] Istituto di Fisica dell'Università, Via Archirafi No. 36, 90123 Palermo. Italy.

0022-4715/85/1000-0201$04.50/0

an intermediate periodic state which, contrary to the assertion in Ref. 13, we suspect plays a very important role.

In this paper we discuss three cases of transitions from tori to fully developed chaos in four- and six-dimensional dissipative dynamical systems in which a (stable) periodic orbit appears in the intermediate regime. This orbit is borne via a tangent bifurcation and the hyperbolic orbit associated to it causes the disappearence of a two-dimensional torus in one case and of a strange attractor in the other two cases through a collision, that is coming in contact with them. The phenomenon seems very much the same as that described as "crisis" in Refs. 14, 15.

The paper is organized in the following way: in Section 2 we introduce concepts and definitions necessary to describe the results contained in Section 3. Finallly, Section 4 is devoted to comments and concluding remarks.

2. CONCEPTS AND DEFINITIONS

All of the models we consider consist of systems of ordinary, first-order, nonlinear differential equations depending on a parameter R. They are obtained under suitable truncations of the Fourier-series expansion of the solution of the Navier–Stokes equations for an incompressible fluid moving on a plane with periodic boundary conditions. The details of the derivations and the specific assumptions used in them can be found in Ref. 16. The models, denoted I, II, and III, respectively, are given explicitly by the following systems:

Model I:

$$\begin{aligned}
\dot{X}_1 &= -X_1 + \sqrt{5}\, X_2 X_4 \\
\dot{X}_2 &= -2X_2 + 4X_3 X_4 + R \\
\dot{X}_3 &= -5X_2 - X_2 X_4 \\
\dot{X}_4 &= -X_4 - \sqrt{5}\, X_1 X_2 - 3X_2 X_3
\end{aligned}$$

Model II:

$$\begin{aligned}
\dot{X}_1 &= -2X_1 + 4X_2 X_3 \\
\dot{X}_2 &= -5X_2 - X_1 X_3 - 9/\sqrt{5}\, X_3 X_4 + R \\
\dot{X}_3 &= -X_3 - 3X_1 X_2 + \sqrt{5}\, X_2 X_4 \\
\dot{X}_4 &= -10X_4 + 4/\sqrt{5}\, X_2 X_3
\end{aligned}$$

Model III:

$$\begin{aligned}
\dot{X}_1 &= -2X_1 + 4X_2X_3 + 4X_4X_5 \\
\dot{X}_2 &= -9X_2 + 3X_1X_3 \\
\dot{X}_3 &= -5X_3 - 7X_1X_2 + R \\
\dot{X}_4 &= -5X_4 - X_1X_5 \\
\dot{X}_5 &= -X_5 - 3X_1X_4 + \sqrt{5}\, X_1X_6 \\
\dot{X}_6 &= -X_6 - \sqrt{5}\, X_1X_5
\end{aligned}$$

All of the models contain only quadratic nonlinearities and depend on the parameter R, which appears in only one of the equations. They exhibit exponential volume contraction: a given volume V_0 at any arbitrary initial time evolves with the law $V(t) = V_0 \exp Ct$, C being the sum of the coefficients of the linear terms of the systems (all negative). Moreover they possess some symmetry properties; in particular I and II are left unchanged if one acts on the variables with the operator

$$\alpha\colon (X_1, X_2, X_3, X_4) \to (-X_1, X_2, -X_3, -X_4)$$

in model II the same happens with the three different operators

$$\begin{aligned}
\alpha\colon\ & (X_1, X_2, X_3, X_4, X_5, X_6) \to (-X_1, -X_2, X_3, X_4, -X_5, X_6) \\
\beta\colon\ & (X_1, X_2, X_3, X_4, X_5, X_6) \to (-X_1, -X_2, X_3, -X_4, X_5, -X_6) \\
\gamma\colon\ & (X_1, X_2, X_3, X_4, X_5, X_6) \to (X_1, X_2, X_3, -X_4, -X_5, -X_6)
\end{aligned}$$

Among α, β, γ the relations $\alpha^2 = \beta^2 = \gamma^2 = \mathbb{1}$; $\alpha\beta = \gamma$, $\alpha\gamma = \beta$, $\beta\gamma = \alpha$ hold. We have mentioned the above symmetries because they have important implications. A set A is symmetric with respct to a symmetry operation σ if, together with any point P, it contains the point $\sigma(P)$. Two sets A and B are symmetrically conjugate under σ if for any point P belonging to A its image $\sigma(P)$ belongs to B and vice versa. As a consequence of the symmetries of our systems any invariant set (periodic orbit, torus, strange attractor) either is symmetric under the symmetries of the model or is bound to occur together with its conjugate partners. Moreover in the presence of symmetries a periodic orbit, besides other types of bifurcations, can undergo that with symmetry breaking: it becomes unstable and at the same time a couple of asymmetric orbits appear close to it. In models I and II the tori we will discuss in the following are symmetric, while in model III we get a couple of them, clearly separated in phase space, transformed into each other by α or β.

A common tool to investigate the evolution (under parameter change) of the tori is provided by the Poincaré sections, that is, the intersection curves produced by the dynamical flow on the two-dimensional torus when the trajectories intersect a given (fixed) hyperplane transverse to them. In general, as is the case in our models I and III, one gets more than one closed curve. The Poincaré sections shown in the following refer, for each model, to a fixed hyperplane and, for the sake of clarity, to a fixed single curve projected on a two-dimensional plane.

Another useful notion to describe the dynamics on a two-dimensional torus is that of rotation number, corresponding to the ratio of the two independent frequencies characterizing the doubly periodic motion. One takes a two-dimensional projection of a Poincaré section, chooses in the interior of a closed curve Γ a fixed point and let it be the origin of a system of polar coordinates. If θ denotes the angular coordinate of a point P on Γ and θ' that of next crossing P', one gets the map f:

$$f\colon\ \theta \to \theta' \qquad \text{or} \qquad \theta' \equiv f(\theta)$$

Taking any initial angle θ_0 on Γ the rotation number associated to it is defined

$$\rho(\theta_0) = \lim_{\nu \to \infty} \frac{1}{2\pi\nu} f^{\nu}(\theta_0)$$

Actually ρ on the torus is independent of θ_0. If θ_0 belongs to a closed periodic orbit one gets

$$\rho(\theta_0) = m/n$$

where n denotes the number of points in which the orbit crosses the section and m the number of full rotations made around the origin when one follows the point with angular coordinate θ_0 back to itself. For details see the references quoted in Ref. 17. We will say that there is a resonance m/n on a torus when the two generally incommensurate frequencies of the motion become rationally related producing a simple periodic motion with an orbit of rotation number equal to m/n.

It is clear that the one-dimensional map $f(\theta)$, although often useful in practice, cannot characterize the motion on the torus faithfully. In fact it contains no information about the other coordinate (amplitude) associated to the projected Poincaré map $P \to P'$.

A different one-dimensional map, better suited to describe the dynamics on the torus, can be constructed using as variable the arc length of the closed curves in the full Poincaré sections. Take again a two-dimensional projection Γ of the intersection of the torus with the fixed hyperplane of the Poincaré section. Choose any point P_0 on it. To any other

point P on Γ associate λ, the arc length (in R^{N-1} if the phase space is R^N) joining P_0 and P on Γ, let us say clockwise. Again the Poincaré map $P \to P'$ defines a one-dimensional map:

$$\varphi\colon \lambda \to \lambda' \qquad \text{or} \qquad \varphi(\lambda) \equiv \lambda'$$

In the following we will refer both to $f(\theta)$ and $\varphi(\lambda)$.

3. RESULTS

Figure 1 (not on scale) summarizes the results concerning model I. The torus $T(A)$ arises via an Hopf bifurcation from the periodic orbit A at $R = C_1$, $232.20 < C_1 < 232.30$. Figure 2 shows its nicely smooth cross section at $R = 235.05$. As R increases further the section of the torus grows in size and at the same time develops four corners which become more and more pronounced. Figure 3a shows that at $R = 240.30$ the four kinks are already very sharp and the trajectory on the torus spend most of the time close to them. A plot of the second iterate of the one dimensional map $f(\theta)$ relative to the curve of Fig. 3a indicate that four fixed points are about to appear (see Fig. 3b). This happens for $R = C_2$, $240.610 < C_2 < 240.615$ when the orbit AT is borne through tangent bifurcation. AT and its symmetric conjugate is shown in Fig. 4. When R approaches C_2 a sequence of resonances is found. The nth resonance has rotation number given by

$$\rho_n = n/(2n+1)$$

Some of these resonances are symmetric, others are not. Figure 5 shows the resonance with rotation number 5/11 and its conjugate, while the following Table gives the values of the parameter R at which some elements of the sequence were found:

3/7	234.9322
4/9	236.84 925
5/11	237.9487
6/13	238.6368
7/15	239.086 11
8/17	239.399 00
9/19	239.627 73
10/21	239.795 50
11/23	239.923 20
12/25	240.023 50
13/27	240.101 70
14/29	240.166 30
15/31	240.217 60

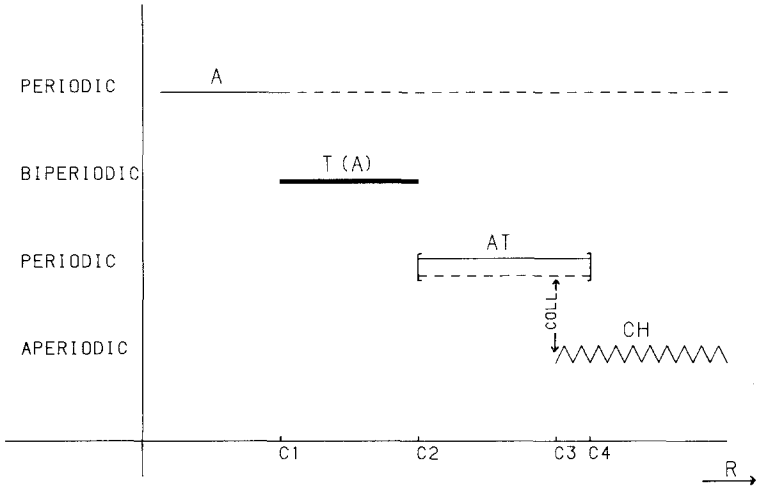

Fig. 1. Schematic picture (not on scale) of the phenomenology found in model I as the parameter R is varied.

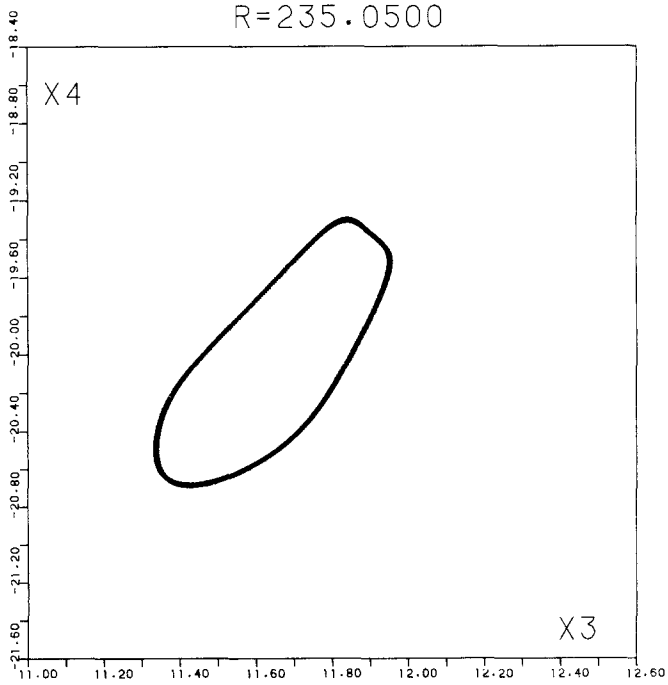

Fig. 2. Projection in the plane X_3–X_4 of the intersection of the torus $T(A)$ with the hyperplane $X_2 = 0$ at $R = 235.050$.

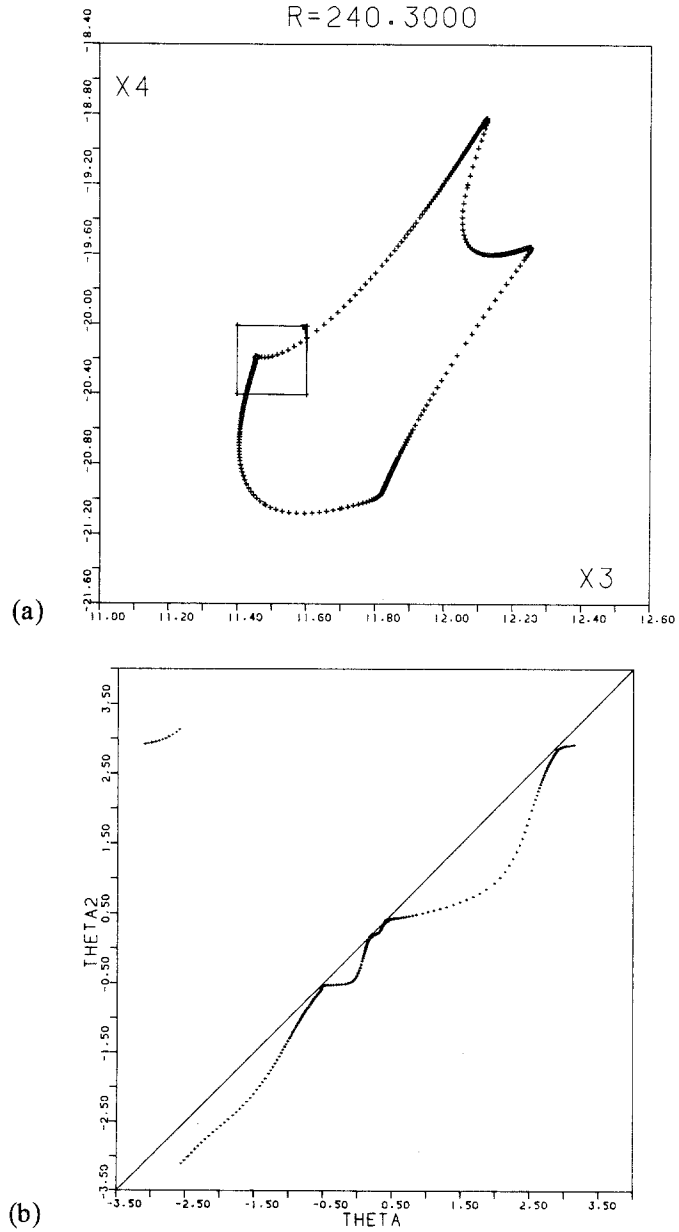

Fig. 3. (a) Projection of $T(A)$ at $R = 240.30$ showing the growth and the changing shape of the torus. (b) Plot of the second iterate of $f(\theta)$ constructed for Fig. 4a taking as origin of the polar coordinates in the plane X_3–X_4 the point (11.75, −20.70); four fixed points (intersections with the line $X_3 = X_4$) are about to appear.

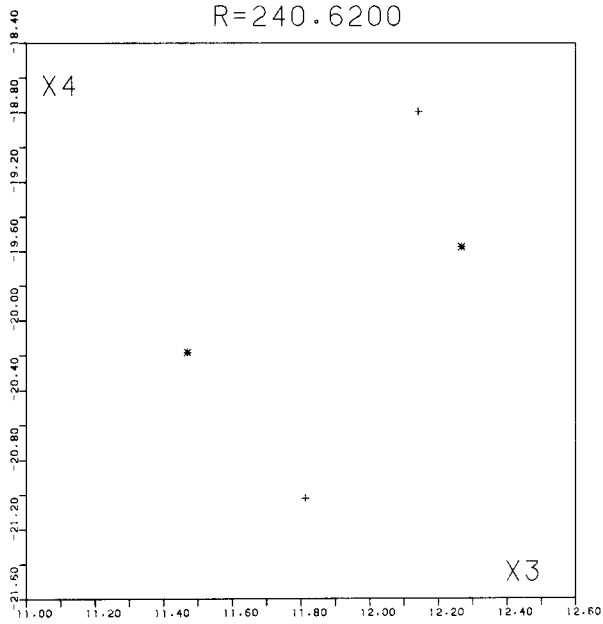

Fig. 4. Projections on the plane X_3–X_4 of the intersections of $AT^r(+)$ and its conjugate (*) with the hyperplane $X_2 = 0$ at $R = 240.620$.

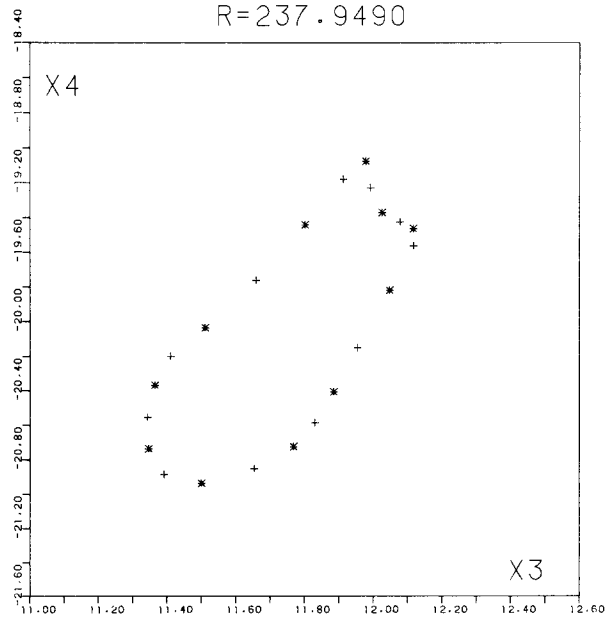

Fig. 5. Resonance with rotation number 5/11 (+) and its symmetrically conjugate (*): projections on the X_3–X_4 plane of the intersections with the hyperplane $X_2 = 0$.

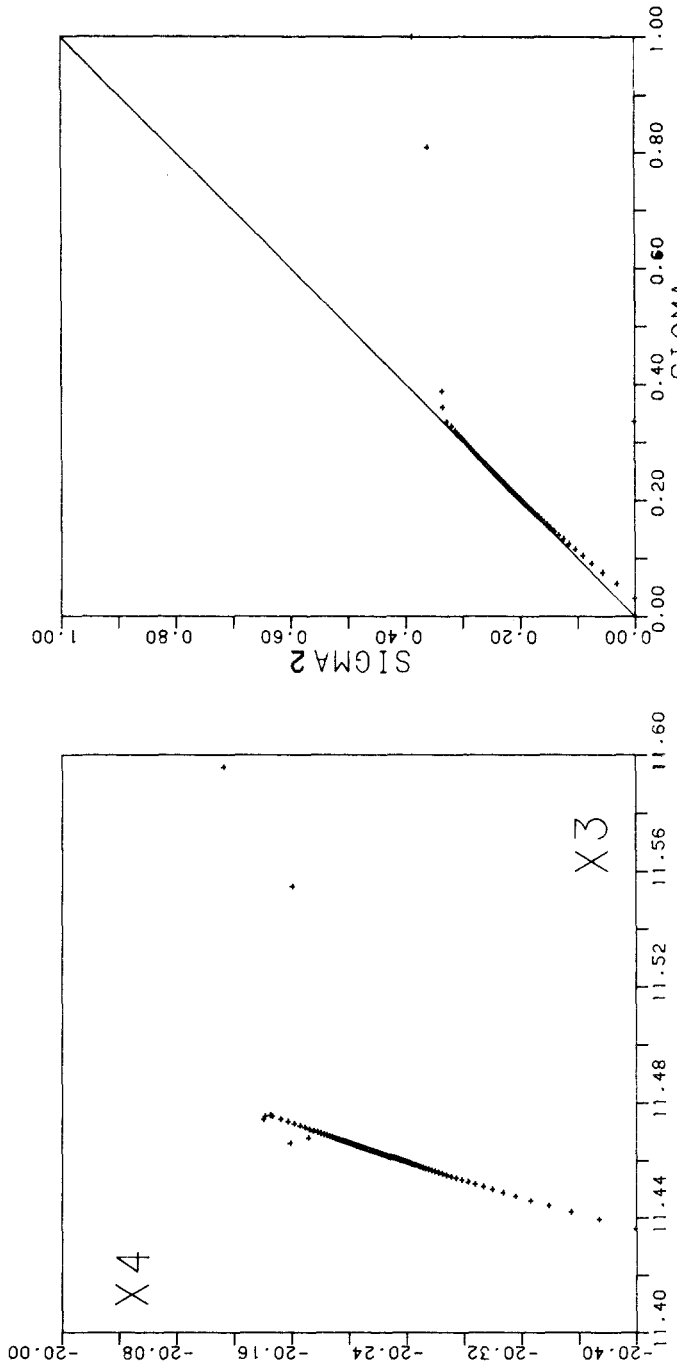

Fig. 6. (a) Enlargment of the inset of Fig. 3a. (b) Second iterate of the function $\varphi(\lambda)$ constructed for the points of Fig. 6a.

The resonances quoted above (and in the following tables as well) are very likely produced and destroyed through saddle node bifurcations; however, owing to their very short lifetime, of the order of 10^{-5} units in the parameter R, we were not able to check this point numerically. Interestingly enough, the orbit AT is exactly the final resonance with rotation number $\rho_\infty = 1/2$ and $C_2 = R_\infty$. From the table above one gets the critical behavior

$$R_\infty - R_n \propto n^{-2}$$

which is very much the same as that reported for one- and two-dimensional maps in Ref. 19 where it is shown to be a consequence of the normal form of the saddle node bifurcation, that is,

$$X' = X + X^2 + \mu$$

with $\mu = R_\infty - R$.

This succession of resonances has already been reported in Ref. 17 where, however, the further approach to chaos of the model was not studied in detail. In order to check that we were actually dealing with a torus up to C_2 we loked at the map $\varphi(\lambda)$ and found that it was indeed invertible until the critical point was reached. Figure 6a shows a portion of the torus corresponding to the inset in Fig. 3a and relative second iterate of $\varphi(\lambda)$ (Fig. 6b). Notice that in this case, because of the little loop in Fig. 6a, $f(\theta)$ would have been noninvertible, suggesting erroneously break-up of the torus.

For parameter values larger than C_3, $252.80 < C_3 < 252.90$, there is a strange attractor shown in Fig. 7a at $R = 253.00$. Some details of its structure are shown in Fig. 7b. Between C_3 and C_4, $253.50 < C_4 < 253.60$, it coexists with the couple of (symmetrically conjugate) orbits we denoted AT. When R decreases from C_4 to C_3 the hyperbolic orbits $(AT)'$ associated to AT become closer and closer to the strange attractor until they collide at C_3. As a consequence of the collision the strange attractor disappears so that between C_3 and C_2 there is no more hysteresis. Figure 7a shows the approach to the collision.

The overall transition from the torus to the strange attractor seems therefore to proceed in two steps: First the sequence of resonances (frequency lockings) on the torus leads to the final locking with $\rho_\infty = 1/2$; the corresponding intermediate periodic regime destroys the aperiodic motion existing at higher values of the parameter when the associated hyperbolic orbits collide with the strange attractor at C_3. The disappearance of chaos through the mechanism of the collision had not been observed yet in Ref. 17. The orbits AT and $(AT)'$ disappear finally through collapse at C_4.

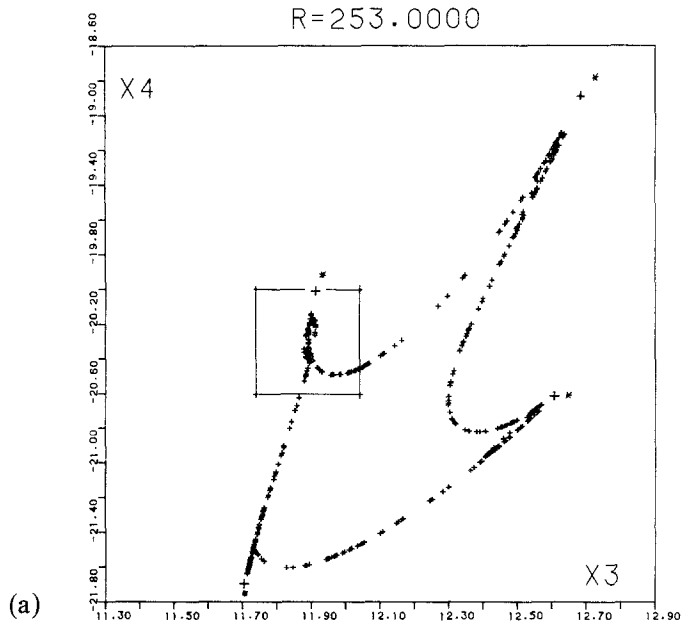

(a)

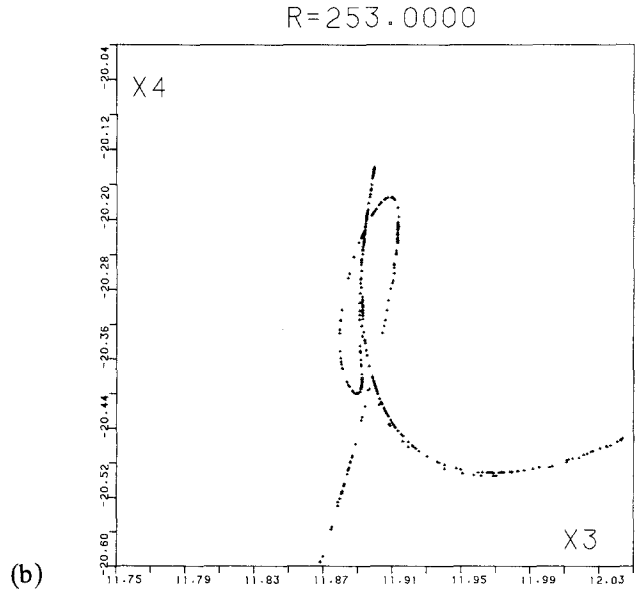

(b)

Fig. 7. (a) Strange attractor at $R = 253.0$ together with the orbit AT at $R = 253.0$ (+) and $R = 253.25$ (*). (b) Enlargment of the inset of Fig. 7a showing the structure of the strange attractor.

Figure 8 summarizes the results for model II. The torus $T(B)$ arises from the periodic orbit B at $R = C_1$, $73.30 < C_1 < 73.50$, via a Hopf bifurcation. The two independent frequencies characterizing the doubly periodic motion have ratio close to 1/5. $T(B)$ initially grows smoothly in size with increasing R. When R increases further the sections develop kinks as shown in Fig. 9a. When $R = C_2$, $75.60 < C_2 < 75.65$, the orbit BT appears together with its hyperbolic partner $(BT)'$ through a tangent bifurcation. In the range of parameter between C_2 and C_3, $75.25 < C_3 < 75.30$, there is hysteresis because of the coexistence of (BT) with another attractor indicated in Fig. 8 as $T(B)$, a two-dimensiona torus. In fact we do not have a biperiodic motion all the way up to C_3. We looked at the one-dimensional map associated to the cross section of the torus when R approaches C_3 and found that the greatest value for which $\varphi(\lambda)$ is invertible is $R = 73.67$. Between $R = 75.68$ and $R = 75.71$ there is a periodic regime with an orbital of rotation number 14/73. At $R = 75.72$, although the intersection curve in the Poincaré section looks very much like that of a torus (see details in Fig. 10) $\varphi(\lambda)$ is not invertible, indicating that we are dealing with a strange attractor. This is confirmed by the computation of the Lyapunov exponents. The toruslike attractor disappears at C_3 when it collides with the hyperbolic orbit $(BT)'$. The approach to the collision is shown in Fig. 9b.

As R increases beyond C_3 $(BT)'$ becomes more and more unstable, while BT at C_4, $75.99 < C_4 < 76.00$ undergoes a symmetry-breaking bifur-

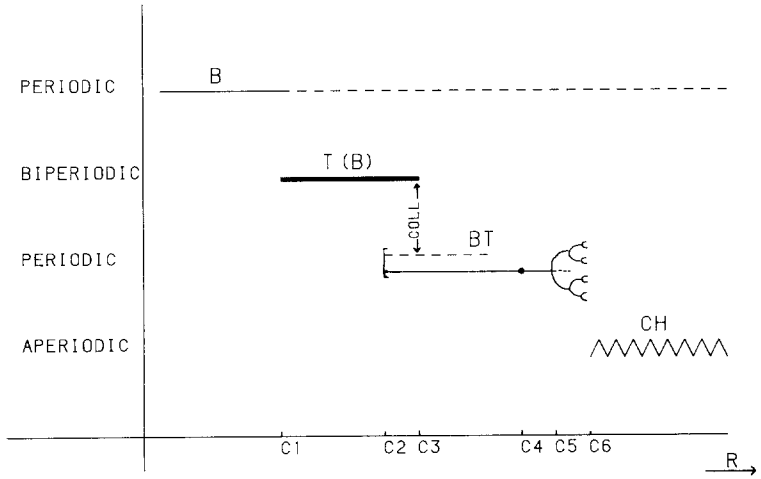

Fig. 8. Schematic picture (not on scale) of the phenomenology found in model II as the parameter R varies.

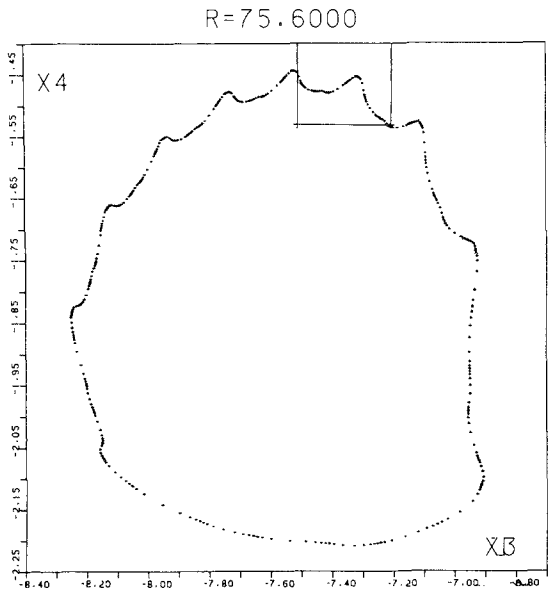

(a)

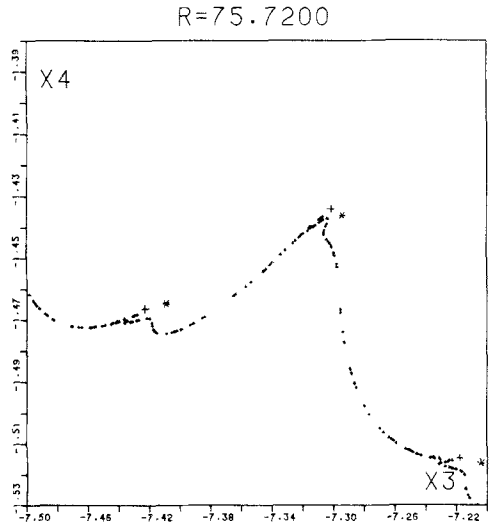

(b)

Fig. 9. (a) Torus $T(B)$ at $R=75.60$. (b) Enlargment of the inset of Fig. 9a showing $T(B)$ at $R=75.72$ together with BT' at $R=75.66$ (+) and at $R=75.72$ (*).

cation. In the schematic Fig. 8 we do not distinguish between BT and $(BT)_{\text{asymmm}}$. This latter (actually the couple of them) at $R = C_5$, $76.01 < C_5 < 76.02$ becomes unstable because of a pitcfork bifurcation followed by a Feigenbaum sequence leading to chaos. Figures 10a–10c, which refer to the same region in phase space shown in Fig. 9b, indicate first the chaotic bands associated to $(BT)_{\text{asymm}}$ and its conjugate, then their merging, and finally full chaos.

As in model I, the intermediate periodic regime of BT provides a link between doubly periodic and fully aperiodic behavior.

Figure 11 shows the resonances 10/51, 15/76, and 20/101 found at R values of 74.360, 74.0425, and 73.873, respectively. They are members of a sequence whose elements appears at the values R_n of the parameter, with rotation number given by

$$\rho_n = n/(5n+1)$$

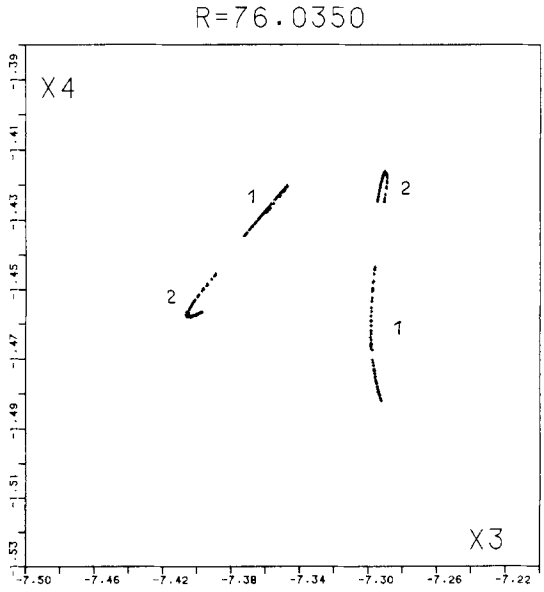

(a)

Fig. 10. (a) Projections of the strange attractor produced by the Feigenbaum sequence of BT (2) and its conjugate (1): pieces present in the same region shown in Fig. 9b. (b) Merging of the pieces 1 and 2 of Fig. 10a. (c) Full chaos.

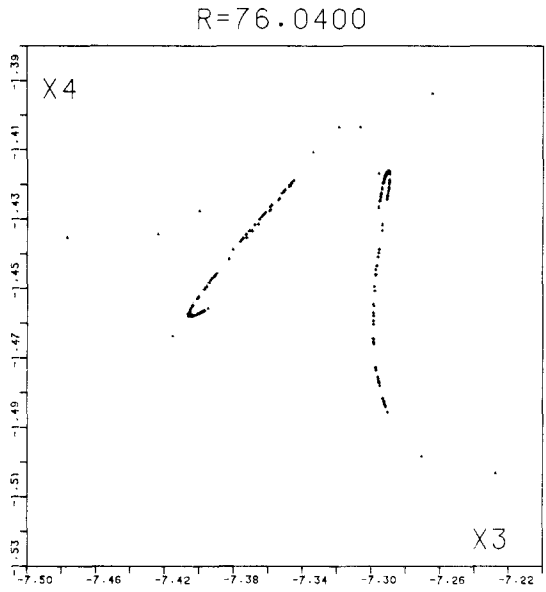

(b)

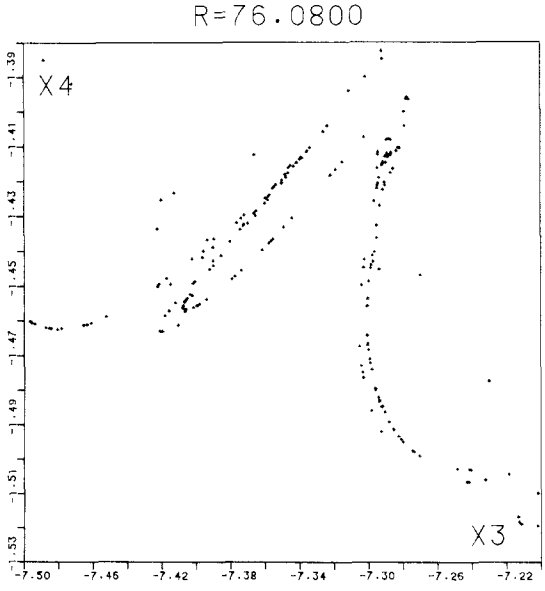

(c)

Fig. 10 (*continued*)

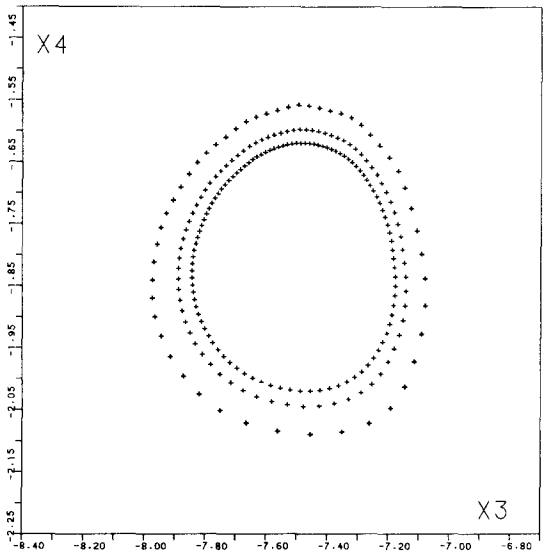

Fig. 11. From outside inward: resonances 10/51, 15/76, and 20/101 on the torus $T(B)$ at $R = 74.360$, 74.0425, and 73.8940 respectively. (Projections on the X_3–X_4 plane of the intersections with the hyperplane $X_1 = 0$.

The following table gives some values of the couples (ρ_n, R_n):

5/26	75.580
6/31	75.130
7/36	74.825
8/41	74.620
9/46	74.470
10/51	74.360
11/56	74.270
12/61	74.195
13/66	74.135
14/71	74.085
15/76	74.0425
16/81	74.0050
17/86	73.9720
18/91	73.9430
19/96	73.9170
20/101	73.8940
21/106	73.8730

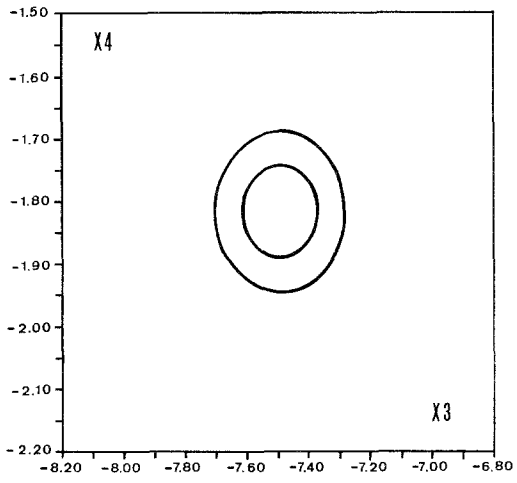

Fig. 12. Torus $T(B)$ at $R = 73.400$ (inside) and $R = 73.55$ (outside).

Note that R_n decreases as n increases. R_∞ occurs at $R = 63.475$, a value of the parameter between C_1 and C_2. The critical behavior indicated by the table above is

$$R_n - R_\infty \propto n^{-1}$$

This critical behavior is different from that encountered in model I, but this is not surprising because in the present case no transition occurs at R_∞. In fact Fig. 12 shows the cross sections of $T(B)$ at an R value slightly smaller (inside) and slightly larger (outside) than R_∞. Figure 13a and 13b show the associated one-dimensional maps given by the fifth iterate of $f(\theta)$ and indicate clearly that at R_∞ it takes the normal form

$$X' = X$$

This means that at R_∞ the torus is spanned by an infinity of resonances with rotation number $\rho_\infty = 1/5$. This degeneracy is clearly due to some symmetry property which is not present for arbitrary values of the parameter but shows up only at R_∞. The origin and nature of this "accidental" symmetry is not clear to us.

The overall transition torus-chaos in model III is shown again schematically and not on scale in Fig. 14. The torus $T(C)$ originates from the periodic orbit C at $R = C_1$, $89.92 < C_1 < 89.93$. As R increases we find

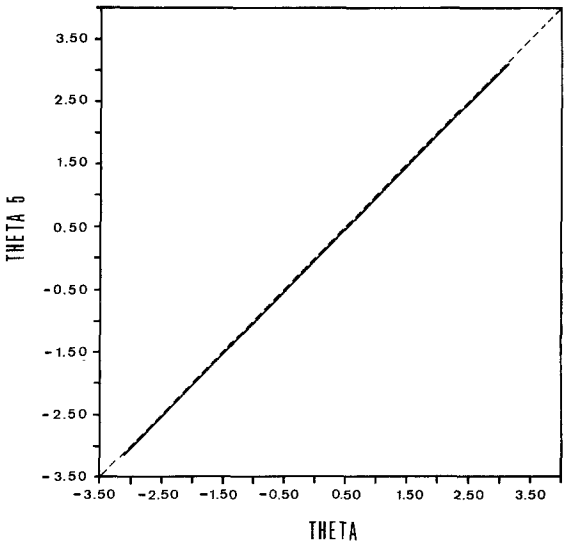

(a)

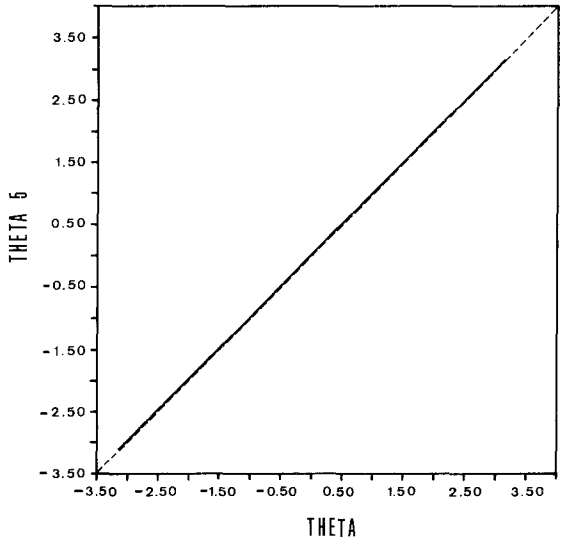

(b)

Fig. 13. (a) Fifth iterate of $f(\theta)$ corresponding to the smaller cross section of Fig. 12. (b) Fifth iterate of $f(\theta)$ corresponding to the larger cross section of Fig. 12.

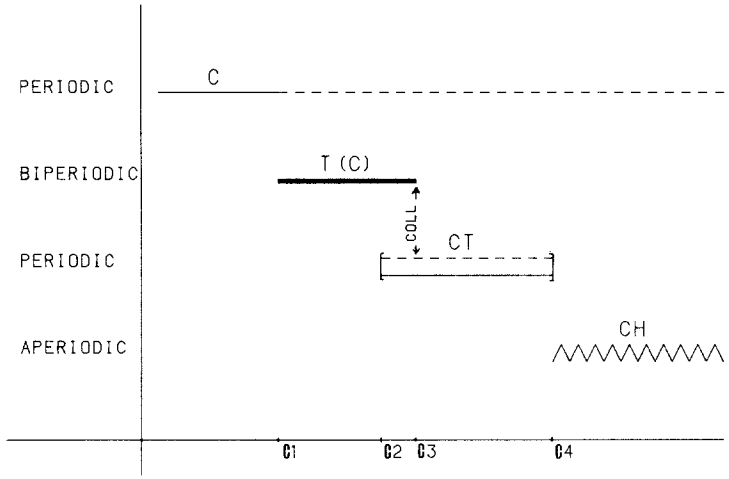

Fig. 14. Schematic picture (not on scale) of the phenomenology found in model III as the parameter R varies.

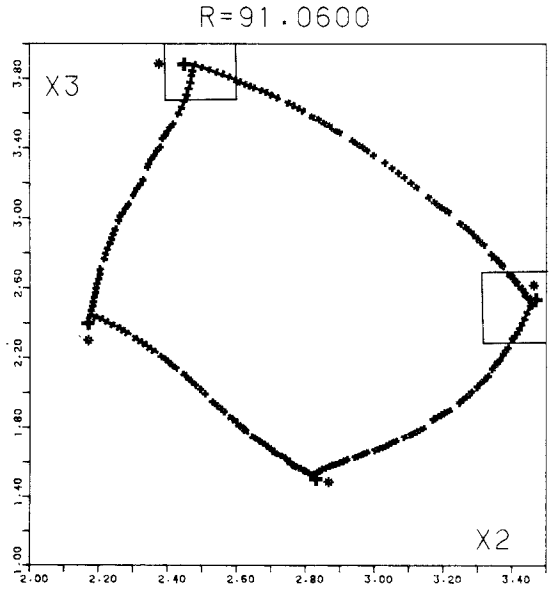

Fig. 15. Projections on the X_2–X_3 plane of the intersection of $T(C)$ with the hyperplane $X_4 = 1.6$ with $R = 91.060$ (+) indicate CT' at $R = 91.06$ (*) CT at $R = 91.00$.

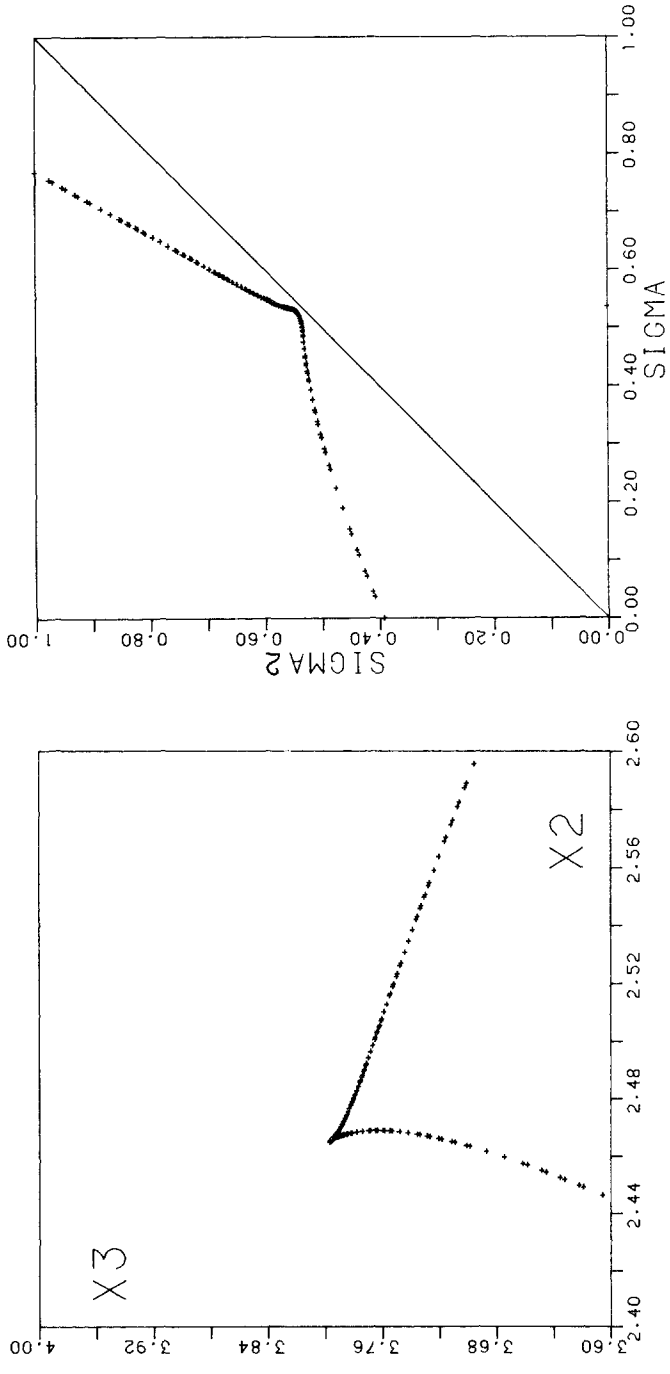

Fig. 16. Enlargment of first inset of Fig. 15, (a); corresponding $\varphi(\lambda)$ map, (b).

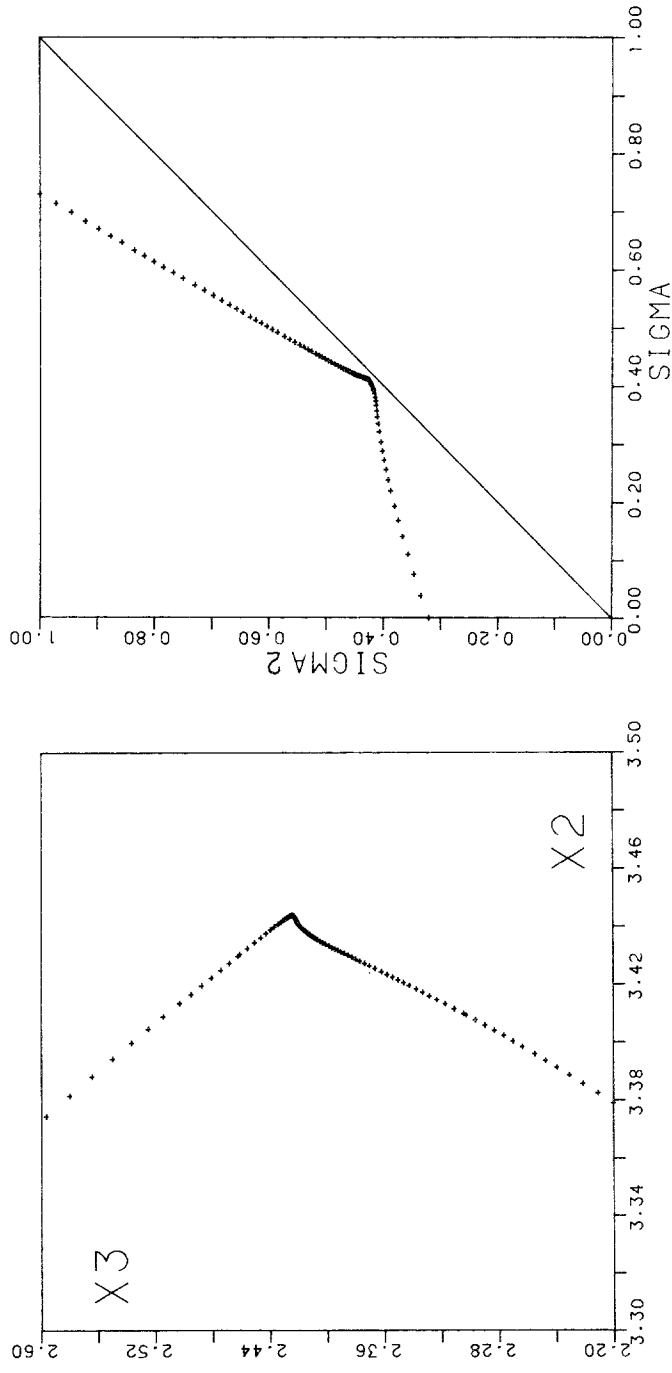

(a) (b)

Fig. 17. Enlargment of second inset of Fig. 15, (a); corresponding $\varphi(\lambda)$ map, (b).

once more that the torus grows in size and begins to develop kinks. At the same time a sequence of resonances is found with rotation numbers

$$\rho_n = n/(2n+1)$$

Some values for the couples (ρ_n, R_n) are given in the following table:

5/11	90.300
6/13	90.550
7/15	90.720
8/17	90.825
9/19	90.898
10/21	90.9485
11/23	90.9835
12/25	91.0070
13/27	91.0235
14/29	91.0350
15/31	91.0427
16/33	91.0480
17/35	91.0520

Between C_2 $(90.95 < C_2 < 90.96)$ and C_3 $(91.06 < C_3 < 91.07)$ the torus coexists with the periodic orbit CT (actually a couple of them, symmetrically conjugate of each other under γ) and its hyperbolic companion $(CT)'$ borne together at $R = C_2$. CT and $(CT)'$ have both rotation number 1/2. At $R = C_3$ $(CT)'$ collides with the torus destroying it. We have used the one-dimensional map φ to check that the doubly periodic motion persists up to the collision point. The approaching collision is also indicated in Fig. 15, while Figs. 16 and 17 show that the one-dimensional map φ is nicely invertible up to $R = 91.061$. The same result has been reported independently in Ref. 18.

Back to the sequence of resonances the critical behavior suggested by the data is

$$R_\infty - R_n \propto \delta^{+n}$$

where $R_\infty = C_3$ and $\delta \cong 0.7$. This behavior differs from the previous two but in this case R_∞ is a critical point in which a collision occurs.

4. CONCLUSION

All of the models described above show the common feature of exhibiting an intermediate periodic regime between an initial doubly periodic and a final aperiodic behavior. In particular it is the hyperbolic

orbit associated to the periodic motion which destroys either a torus or a strange attractor. On the other hand the sequence of resonances found on the tori have different critical behavior: in model I R_∞ corresponds to the sharp transition torus-periodic orbit via final frequency locking and $(R_\infty - R_n)$ goes like an inverse square with n. In model II R_∞ corresponds to a normal, smoth biperiodic regime and one finds simple $1/n$ decrease. Finally in model III R_∞ is a collision point and we get power law δ^n. One could ask oneself if the critical behavior in models I and III belongs to nontrivial universality classes. As for model I the results of Refs. 19 and 20 suggest that this could be the case. For model III the question seems open. There are in fact similar results in some recent literature dealing with breakdown of tori in dissipative systems (see Refs. 23–25) but the connections with our cases are not obvious to us. The collision mechanism found in our models has been reported independently also in Ref. 18. We are inclined to believe that it could show up under closer examination also in the systems considered in Refs. 13, 21, and 22. The analogy with the "crisis" events of Ref. 14 is very striking but probably more experimental (numerical) evidence and theoretical work are needed to appreciate fully its genericity and relevance in the behavior of dynamical systems.

ACKNOWLEDGMENTS

We are indebted to Prof. G. Gallavotti for useful comments on a previous version of this work and for having suggested to us the use of $\varphi(\lambda)$. Our thanks are also due to the Director and the Staff of the Computer Center of the University of Palermo for assistance during the numerical computations.

This work was partially supported by GNFM (Gruppo Nazionale di Fisica Matematica) and the Italian Ministry of Public Education, M.P.I.

REFERENCES

1. J. P. Eckmann, *Rev. Mod. Phys.* **53**:643 (1981).
2. P. Collet and J. P. Eckmann, *Iterated Maps on the Interval as Dynamical Systems*, (Birkhauser, Basel, 1980).
3. R. H. Helleman, in *Fundamental Problems in Statistical Physics*, Vol. V, E. G. Cohen, ed. (North-Holland, Amsterdam, 1980).
4. R. H. Helleman, in *Long Time Predictions in Dynamics*, W. Horton, L. Reichel, and V. Szbehely, eds. (Wiley, New York, 1982).
5. E. Thoulouze-Pratt and M. Jean, *Int. J. Non-linear Mech.* **17**:319 (1982).
6. V. Franceschini, *Physica* **6D**:285 (1983).
7. A. Arneodo, P. H. Coullet and E. A. Spiegel, *Phys. Lett.* **94A**:1 (1983).
8. K. Kaneko, *Prog. Theor. Phys.* **69**:1806 (1983).

9. H. Fujisaka and T. Yamada, *Phys. Lett.* **66A**:66 (1978).
10. J. H. Curry, *Commun. Math. Phys.* **60**:60 (1978).
11. D. G. Aronson, M. A. Chory, G. R. Hall and R. P. McGehee, *Comm. Math. Phys.* **83**:303 (1982).
12. J. H. Curry and J. R. Johnson, *Phys. Lett.* **92A**:217 (1982).
13. J. H. Curry and J. A. Yorke, *Lecture Notes in Mathematics* No. 668 (Springer, New York, 1978).
14. C. Grebogi, E. Ott and J. A. Yorke, *Phys. Rev. Lett.* **48**:1507 (1982).
15. C. Grebogi *et al.*, University of Maryland preprint, 1982.
16. P. M. Angelo and G. Riela, *Nuovo Cimento* **64B**:207 (1981).
17. G. Riela, *Z. Phys.* **54B**:187 (1984).
18. V. Franceschini and C. Tebaldi, *Commun. Math. Phys.* **94**:317 (1984).
19. K. Kaneko, *Prog. Theor. Phys.* **68**:669 (1982).
20. K. Kaneko, *Prog. Theor. Phys.* **69**:403 (1983).
21. J. R. Beddington, C. A. Free and J. H. Lawton, *Nature* **255**:58 (1975).
22. I. Schreiber and M. Marek, *Phys. Lett.* **91A**:263 (1982).
23. S. J. Shenker, *Physica* **5D**:405 (1982).
24. M. J. Feigenbaum, L. P. Kadanoff, and S. J. Shenker, *Physica* **5D**:370 (1982).
25. S. Ostlund, D. Rand, J. Sethna, and E. Siggia, *Physica* **8D**:303 (1983).